Mat. Res. Soc. Symp. Proc. Vol. 692 © 2002 Materials Research Society

Quantum dots of InAs/GaSb type II superlattice for infrared sensing
(Invited paper)

M. Razeghi [a], Y. Wei, A. Gin
Northwestern University, Center for Quantum Devices, ECE Department
Evanston, IL 60208

G. J. Brown
Air Force Research Laboratory, Materials & Manufacturing Directorate, AFRL/MLPS,
Wright-Patterson AFB, OH 45433-7707

ABSTRACT

Throughout the past years, significant progress has been made in Type II (InAs/GaSb) photovoltaic detectors in both LWIR and VLWIR ranges. BLIP performance at 60K for 16μm photovoltaic type II detectors has been successfully demonstrated for the first time. The detectors had a 50% cut-off wavelength of 18.8 μm and a peak current responsivity of 4 A/W at 80K. A peak detectivity of 4.5×10^{10}cm·Hz$^{1/2}$/W was achieved at 80K at a reverse bias of 110mV. Detectors of cutoff wavelength up to 25μm have been demonstrated at 77K. The great performance of single element detectors appeals us to lower dimensional structures for both higher temperature performance and possible wavelength tunability. Simple calculations show that quantum effects will become significant when the lateral confinement is within tens of nanometers. The variation of applied gate voltage will move the electron and hole energy levels unevenly. The cutoff wavelength of the superlattice will vary accordingly. Auger recombination will also decrease and higher temperature operation becomes possible. In this talk, the latest results will be discussed.

INTRODUCTION

In recent years, extensive research has been done on infrared photodetectors for use throughout the mid to very long wavelength (3-25μm) range. These detectors have a wide variety of military, medical, and industrial applications. Uncooled infrared (IR) detectors are required for low-cost, lightweight sensor applications. Commercially available uncooled IR devices use ferroelectric or microbolometer detectors. These sensors are inherently slow and cannot detect rapid signal changes needed for many applications. Some of the applications which require a fast detector response time ($\tau < 30$ msec) are: free-space communication, proximity fuses, active infrared countermeasure systems, non-invasive medical monitoring, and LIDARs. Although photon detectors have frequency responses in the megahertz range, their high temperature detectivity is severely degraded due to physical limitations. The existing infrared photon detectors can be categorized as interband, which are mostly HgCdTe and InAsSb, or intersubband quantum well infrared detectors (QWIP)[1]. Unfortunately, fast Auger recombination rate in such interband detectors[2] and high thermal generation rate in the

[a] Electronic mail: razeghi@ece.northwestern.edu

intersubband detectors decrease their performance for room temperature operation drastically.

As another alternative for infrared photodetectors, type-II superlattices have been studied which were originally suggested by Sai-Halasz and L. Esaki[3]. In order to realize Auger suppression at room temperature, we have developed a new type-II superlattice detector design[4]. The experimental results show nearly one order of magnitude lower Auger recombination rate at room temperature in such detectors compared to typical intrinsic (HgCdTe) detectors with similar bandgap. Type II detectors based on InAs/GaSb superlattices have shown the potential to be the next generation of infrared sensors, surpassing HgCdTe performance over a wide range of optical wavelengths. In the VLWIR range, photodiodes based on type II InAs/GaSb superlattices with a 16μm 50% cutoff wavelength were reported with a detectivity of 1.5×10^{10}cmHz$^{1/2}$/W at 80K[5]. Photodiodes with a 22μm cutoff wavelength have also been demonstrated at 80K[6]. Most recently, 18.8μm photodiodes have shown a detectivity of 4.5×10^{10}cmHz$^{1/2}$/W at 80K with moderate bias of −110mV[7]. This will be discussed in more detail below. In addition, uncooled detectors with cutoff wavelengths between 8-12μm have been fabricated[8]. Single-element detectors[9] show a detectivity of 1.3×10^{8} cmHz$^{1/2}$/W at 11μm at room temperature which is comparable to microbolometers under similar conditions. However, the measured response time of the detector is less than 68 nsec which is more than six orders of magnitude faster than microbolometers.

With the promising performance of single element detectors, researchers are attempting to increase electron confinement and wavelength tunability by moving to detectors that make use of quantum dots. Most recently in this field, others are making self-assembled quantum dot infrared photodetectors (QDIP). The dots are formed in Stranski-Krastanow growth mode in MBE. These detectors make use of the intersubband transition for detection in the wavelength range of 8~12μm. Peak detectivity, D* of 3×10^{9} cmHz$^{1/2}$/W at 100K has been reported[10]. Instead of using random self-assembled growth techniques, we plan to use electron beam lithography to create regular arrays of quantum dot infrared detectors. In this paper, we show some preliminary results towards this goal.

EXPERIMENT

The type II InAs/GaSb superlattice material is grown by an Intevac Modular Gen II molecular beam epitaxy equipped with As and Sb valved cracker sources on *p*-type epi-ready GaSb substrates. This material is used for large area detectors. The photodiode structures were grown at 396 °C according to a calibrated pyrometer. First, a 0.75μm GaSb buffer layer doped with Be (p~1×10^{18} cm^{-3}) was deposited. Then, InAs/GaSb:Be (p~1×10^{18} cm^{-3}) superlattice was grown, followed by a nominally undoped superlattice. Finally, InAs:Si/GaSb (n~1×10^{18} cm^{-3}) superlattice was grown and capped with InAs:Si (n~1×10^{18} cm^{-3}) top contact layer. The growth rate was 0.5 monolayer/s for InAs layers and 0.8 monolayer/s for GaSb layers. The V/III beam-equivalent pressure ratio was about 4 for InAs layers and about 1.2 for GaSb layers. The cracker temperature for As and Sb cells was 800°C. The improved material growth was achieved by greatly reduced lattice mismatch between the superlattice and the substrate, as well as reducing the growth

temperature for the n-type superlattice layers. The selected layer numbers of InAs and GaSb layers were determined for specific cutoff wavelengths using an empirical tight binding model. The lattice mismatch was predicted by the weighted average lattice constants of InAs, InSb and GaSb. InSb lattice constant is used for the interfaces between InAs and GaSb layers. For devices with a cutoff wavelength of nearly 19μm at 80K, we used 17 InAs monolayers and 7 GaSb monolayers for each superlattice period. The predicted 50% cutoff wavelength that is 18μm at 77K closely agrees with the experimental results.

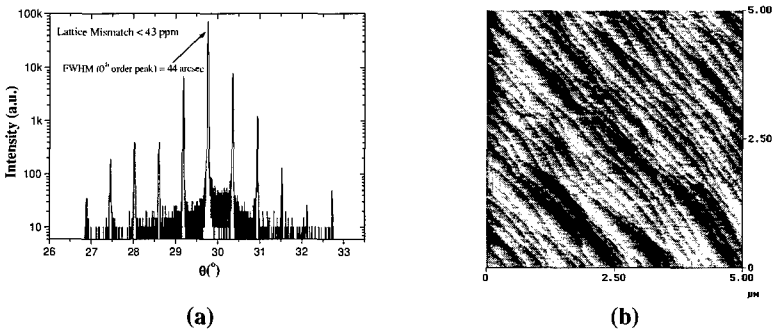

(a) **(b)**

Figure 1. (a) High resolution X-ray diffraction of high quality InAs/GaSb superlattice. The lattice mismatch between the superlattice and the substrate is almost zero. **(b)** AFM image of the sample surface over 5μm×5μm. Smooth atomic steps are very clear.

Structural quality of the epitaxial layers was assessed using a Phillips high-resolution x-ray diffraction system. Figure 1(a) shows the typical x-ray diffraction pattern of the photodiode structures. The mismatch between the average lattice constant of the superlattice and the GaSb substrate is below 0.0043%, while the full width at half maximum (FWHM) of the zeroth order peak is below 45 arcsec for the grown devices. The surface morphology of the samples was studied with a Digital Instruments Nanoscope IIIa atomic force microscope (AFM). The theoretical study[11] as well as experimental results[12] show the strong correlation between the surface roughness and the performance of InAs/$Ga_{1-x}In_xSb$ superlattice photodiodes. We have achieved a root mean square (RMS) surface roughness below 1.6Å over an area of 20μm×20μm, which is the record for the type II InAs/$Ga_{1-x}In_xSb$ material system. Figure 1(b) shows the gray-scale surface morphology of a sample. Clear and smooth atomic steps are visible over the 5μm×5μm scan area and indicate excellent surface smoothness.

The processed detectors were attached to the cold finger of a LakeShore Cryogenics helium cryostat with KRS-5 windows. The temperature was controlled precisely between 20K and 100K. Absolute spectral responsivity was calculated from the measured spectral response of the device using the Mattson Galaxy 3000 Fourier transform infrared (FTIR) spectroscopy system, and its photoresponse to a calibrated blackbody (Mikron 305) setup.

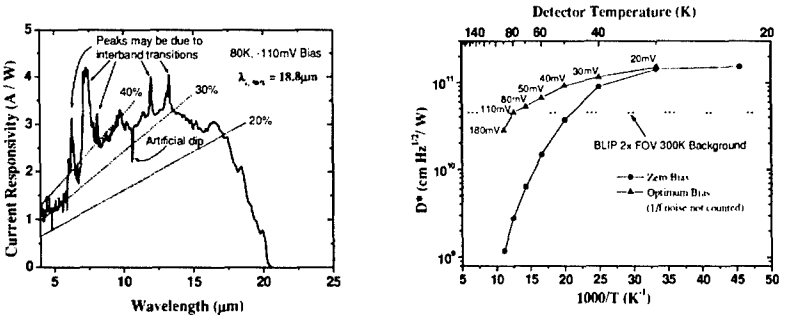

(a) (b)

Figure 2. (a) Absolute current responsivity of the detectors at 80K under a reverse bias of 110mV. The dotted lines are equal-quantum efficiency lines. The 90% to 10% cutoff energy width is about 12meV. **(b)** Temperature dependent peak detectivity at 12 μm (50% cutoff is at 18.8 μm at 80K) with optimum bias and zero bias. With a reverse bias of 110mV, BLIP performance can be achieved at 80K.

Figure 2(a) shows the typical spectral responsivity of the detectors with $\lambda_{c,50\%}$ = 18.8μm. The absorption from CO_2 and H_2O due to the small difference in the optical path length of the background measurement and the detector measurement is corrected from the measurements of the air transmission. The peak responsivity for the sample is about 4A/W under a bias of -110mV at 80K which leads to a quantum efficiency of 41.4% at 12μm. The quantum efficiency of the detectors is obtained by dividing the current responsivity by its theoretical value which is given by,

$$R_{i,theoretical} = \frac{\eta_{ideal}\lambda e}{hc}, \quad \text{with } \eta_{ideal} = 1$$

where λ is the wavelength, e is the electron charge, h is the Plank's constant, and c is the speed of light in the air. The use of binary layers in the superlattice has significantly enhanced the uniformity and reproducibility of the energy gap. The 90% to 10% cut-off energy width of these devices is only about 2 kT, which has been maintained very well compared with previous detectors operating at different cutoff wavelength[5].

The major noise component at zero bias is the Johnson noise, and hence the detectivity of the device with current responsivity Ri at temperature T can be calculated from:

$$D^* = R_i\sqrt{\frac{R_0 A}{4kT}}$$

where R_0 is the zero bias differential resistance of the device, A is the device area, and k is the Boltzmann constant. The measured value for R_0A product for the detectors was about 0.27Ωcm^2 at T = 50K which leads to a Johnson noise limited detectivity of about 3.71×10^{10}cm·Hz$^{1/2}$/W. Under reverse bias, the 1/f noise will show up. However with appropriate modulation frequency, this noise can become negligible. The RA product goes up to 0.55Ωcm^2 at 80K and a reverse bias of 110mV. This lead to a Johnson noise

limited detectivity of 4.5×10^{10}cm·Hz$^{1/2}$/W. Figure 2(b) shows the calculated detectivity with optimum reverse bias at different temperatures without the 1/f noise component compared with those under zero bias. The background limited infrared photodetector (BLIP) level is achieved at temperatures near 50K under zero bias and 80K under a reverse bias of 110mV.

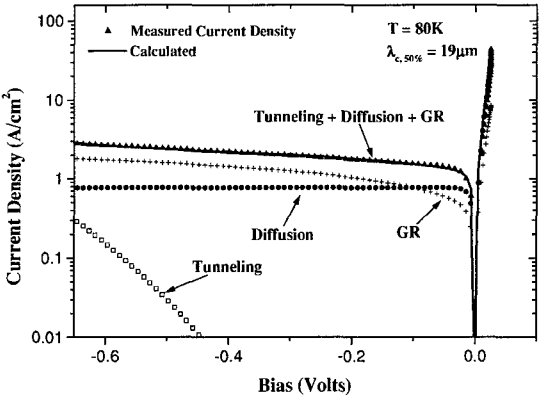

Figure 3. Comparison between measured dark current density and modeled dark current density components at 80K. At reverse bias below 100mV, the dominant dark current is the diffusion current.

The 50% cutoff wavelength decreases from 19.1μm at 90K to 17.6μm at 20K representing the temperature-dependent changing in bandgap of 5.5meV. For HgCdTe detectors of a similar cutoff wavelength, this change is about 23meV in the opposite direction and more than four times larger, calculated from Ref. [13]. In order to study the major components of the dark current at T = 80K, the current–voltage characteristic of the devices was modeled. Although the active layer of these devices consists of short period superlattices, bulk-based modeling of the dark current has been proven to give relatively accurate results [8,14,15]. We use an improved algorithm and more accurate calculations from Matlab based on formalism reported in Ref. [8]. Figure 3 shows the measured and modeled current densities versus the applied bias for devices with $\lambda_{c,50\%}$ = 18.8μm. The calculated current density, which consists of tunneling, generation recombination, and diffusion current densities, shows good agreement to the measured values for forward and reverse biases. We assumed an effective mass of m_e=0.03m_0 for electrons and m_h=0.4m_0 for holes based on previous theoretical calculations[11] and experimental results[14,16]. Based on the experimental measurements on similar devices[17], we also assumed an electron mobility parallel to the growth direction of μ_e=1000 cm^2/Vs. The mobility of the holes is not significant in the diffusion current, since the device has an n^+-p junction. The fitting parameters for the model were carrier lifetime $\tau_e = \tau_h$=24ns, unintentional background doping level $p\sim1\times10^{15}$cm^{-3}, and generation-recombination lifetime in the depleted layer of τ_{gr} = 0.4ns. In contrast to

HgCdTe, tunneling is not significant even at high values of the reverse bias due to the higher effective mass of the electrons in type-II superlattices. At low reverse bias, the dark current is dominated by diffusion current at 80K. The generation-recombination current begins to take over at reverse bias over 100mV. The value of R_0A product versus temperature shows a diffusion limit behavior down to nearly 50K, and then a generation-recombination limit behavior from 50K to 35K. Below 35K, the value of R_0A increases even slower. The ideality factor of the device was nearly 1 for small values of forward bias at 80K.

These large area detector results encourage us to move forward towards higher performance quantum dot devices. We pursued a novel method unlike the commonly used "self assembled" technique that can produce high quality, highly uniform quantum dot structures using electron beam lithography. These detectors use interband transitions in type II InAs/GaSb superlattice materials to achieve higher operating temperatures. The type II band alignment in between InAs layers and GaSb layers directly lead to lower Auger recombination rate. As the semiconductor dots get smaller, usually in tens of nanometer, the quantum confinement effect will become significant and energy levels will become increasingly discrete. This will decrease the matching energy levels for Auger recombination dramatically and much higher operating temperatures could be achieved. The material structure is shown in Figure 4(a). By using gate electrodes to apply a lateral electrical field to the detector, we can further confine the electrons in space, which changes the available energy states in the quantum dot. By assuming a parabolic potential well formed by the gate voltage, we can calculate the electron energy level shift as a function of gate bias voltage, shown in Figure 4(b). Consequently, we can control the detector cutoff wavelength by several microns by using applied voltages on the order of one volt as shown for different sized detectors in Figure 5. Also no surface grating is necessary for these quantum dots. This reduces some of the processing steps and, therefore, detector cost. This is a completely new technique to realize quantum dots.

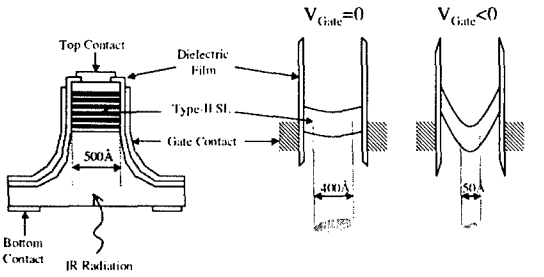

Figure 4. **(a)** Schematic diagram of one possible structure of the proposed quantum dot infrared detector; **(b)** The basic operating mechanism.

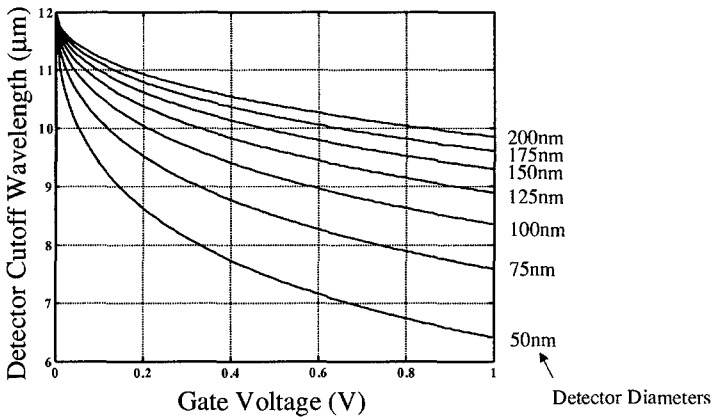

Figure 5. Preliminary modeling results for the wavelength tunability for quantum dots of various diameters.

Although the basic idea of these detectors seems elementary, the fabrication techniques needed are of critical importance. The processing for nanometer sized features is a challenge. The starting material is a type II InAs/GaSb superlattice. Stacks of high quality quantum dots can be developed by etching pillars and consequent oxide coating. In order to achieve quantum size effect, one needs to confine the electrons within tens of nanometer. However, surface leakage current will be a severe problem for such a small device, since the ratio of the surface to the volume increases dramatically. However by applying a gate voltage, not only can the cutoff wavelength be changed, the electrons will also be more confined to the center and result in less leakage.

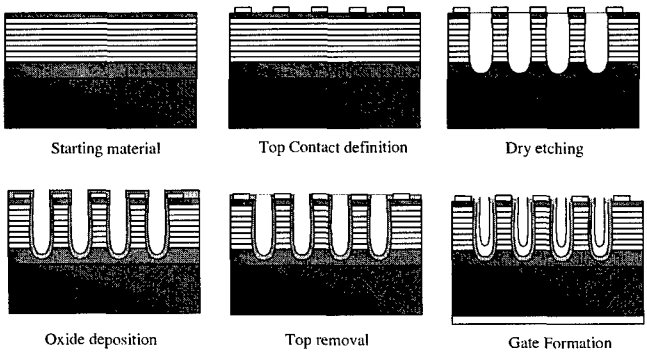

Figure 6. Interconnection of the pillars with advanced metalization and passivation techniques.

The sensitive area of such quantum pillar is very small and many detectors need to be combined to serve as a single detecting pixel. Figure 6 shows the interconnection scheme which provides a large detector area using advanced metalization and passivation techniques. A Leica LION-LV1 low energy e-beam lithography system was used to produce top metal contacts. High quality metal contacts with diameter in the range of 1000 to 100nm were successfully defined on the surface of the samples. Reactive ion etching (RIE) was used to produce uniform anisotropic etching of the pillars through the material. The etching was designed for high ratio of vertical to horizontal etching rates. Figure 7(a) shows the results of such process on the 500nm diameter pillars. The vertical to horizontal ratio is in excess of five. We have produced two-dimensional arrays of this pillars with excellent uniformity over thousands of square micron. Additionally, electron beam lithography was used to create 40nm diameter holes in PMMA resist, demonstrating our high-resolution capability. The atomic force microscope scan is shown in Figure 7(b).

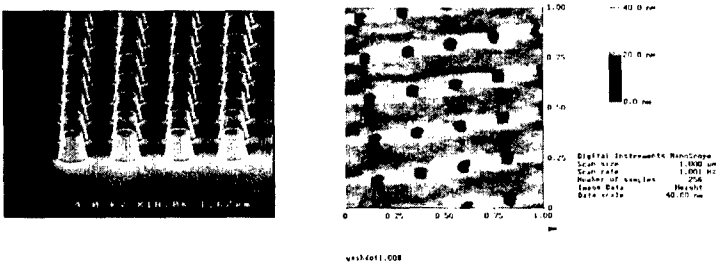

(a) (b)

Figure 7. Current progress in processing technology. (a) Etched array of 500nm GaSb dots; (b) AFM image of 40nm diameter holes in PMMA/GaSb

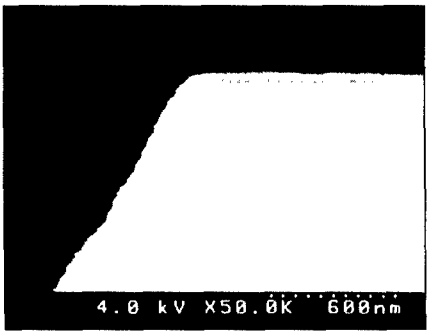

Figure 8. SEM image of the cleaved edge of a mesa covered by a uniform layer of dielectric with a thickness of about 50nm.

Passivation is one of the most important steps to control surface-induced leakage current. Surface leakage originates from unterminated, or dangling, bonds at the surface of a semiconductor. When the tetrahedral GaSb or InAs lattice is abruptly terminated along a given plane to form a surface, some of the crystal's bonds are left dangling. The formation of a native oxide terminates most of the unsatisfied bonds, but the remaining dangling bonds become interfacial traps. These traps introduce energy levels in the forbidden band gap at the semiconductor-oxide interface. They tend to pin the Fermi level near mid-bandgap and create surface leakage current. In addition, In_2O_3, the native oxide formed on InAs or InSb, is a good conductor, which acts to decrease the resistance for the leakage path in photodiode and photoconductor devices. Therefore we need to remove the native oxides and deposit or grow a layer of insulating material to terminate all the dangling bonds and protect the surface. The key issues are the uniformity of the dielectric and the coverage of the device surface. We used plasma enhanced chemical vapor deposition (PECVD) techniques to form uniform layers of dielectrics. Figure 8 shows SEM image of a cleaved edge of a mesa covered with 50nm Si_3N_4 layer by this method.

Most of the remaining challenges with this approach are processing related. For instance, metal liftoff, the standard process for forming metal contacts, is slightly different for mesa diameters below 100nm. The surface adhesion is minimal over the small detector area and the evaporated contacts tend to peel off with the rest of the metal layer. Additionally, etching the nanopillars needs to be very carefully controlled with small devices. It becomes more challenging to achieve high aspect ratio structures by techniques such as reactive ion-etching, because the high energy plasma tends to isotropically etch at small dimensions. However, technologies will be improved to overcome these difficulties.

CONCLUSION

We have demonstrated the initial success for the processing technology of quantum dot arrays on GaSb substrates. Highly uniform dots formed by electron beam lithography have been successfully realized. Surface passivation by depositing silicon nitride has also been studied. Because the quantum confinement effects lead to much lower Auger recombination rates, this work may lead to a new generation of infrared detectors operating at much higher temperatures than previous technologies.

ACKNOWLEDGEMENTS

This work has been partially supported by Air Force and the Office of Naval Research. The authors would like to acknowledge the support of Dan Johnstone of Air Force and Y. S. Park of ONR. A. Gin is supported under a National Science Foundation Graduate Research Fellowship.

REFERENCES

1. M. A. Kinch and A. Yariv, Appl. Phys. Lett. **55**, 2093, 1989.
2. A. Rogalski, Infrared Physics & Technology **40**, 279, 1999.

3. G. A. Sai-Halasz, R. Tsu, and L. Esaki, Appl. Phys. Lett. **30**, 651, 1971.
4. H. Mohseni, E. Michel, J. Sandven, M. Razeghi, W. Mitchel, and G. Brown, Appl. Phys. Lett. **71**(10), 1403, 1997.
5. H. Mohseni, M. Razeghi, G.J. Brown, Y.S. Park, Appl. Phys. Lett., **78**(15), 2107-2109, 2001.
6. Hooman Mohseni, Yajun Wei and Manijeh Razeghi, Proc. SPIE, **4288**, 191-199, 2001.
7. Y. Wei, A. Gin, M. Razeghi, and G. Brown, submitted to Appl. Phys. Lett., Oct. 2001.
8. Hooman Mohseni, Joseph S. Wojkowski, Abbes Tahraoui, Manijeh Razeghi, G. Brown, and W. Mitchel, Proc. SPIE, **3948**, 153-160, 2000.
9. H. Mohseni, J. Wojkowski, M. Razeghi, IEEE J. Of Quantum Elect. **35**, 1041, 1999.
10. A. D. Stiff, S. Krishna, and P. Bhattacharya , Appl. Phys. Lett., **79**(3), 2001.
11. G. Bastard, Phys. Rev. B **25**, 7584 (1982).
12. F. Fuchs, L. Burkle, W. Pletschen, J. Schmitz, M. Walther, H. Gullich, N. Herres, and S. Mueller, Proc. SPIE **3794**, 41 (1999).
13. W.M. Higgins, G. N. Pultz, R.G. Roy, R.A. Lancaster and J.L. Schmit, J. Vac. Sci. Technol. A **7** (2), 271 (1989).
14. J. L. Johnson, L. A. Samoska, A. C. Gossard, J. Merz, M. D. Jack, G. R. Chapman, B. A. Baumgratz, K. Kosai, and S. M. Johnson, J. Appl. Phys. **80**, 1116 (1996).
15. F. Fuchs, U. Weimar, E. Ahlswede, W. Pletschen, J. Schmitz, and M. Walther, Proc. SPIE **3287**, 14 (1998).
16. F. Fuchs, U. Weimar, W. Pletschen, J. Schmitz, E. Ahlswede, M. Walther, J. Wagner, and P. Koidl, Appl. Phys. Lett. **71**, 3251 (1997).
17. L. Burkle, F. Fuchs, R. Kiefer, W. Pletschen, R. E. Sah, and J. Schmitz, Mater. Res. Soc. Symp. Proc. **607**, 77 (2000).